AIAA 80-1310R

MX Missile Thermal Mapping and Surface Flow Results

W.J. Maegley* and H.R. Carroll†
Martin Marietta Corporation, Denver, Colo.

Results of wind tunnel tests to determine aerodynamic heating patterns and general flowfield characteristics on the MX missile are discussed. 5% and 12½% scale models of the missile configuration were tested at Mach 6 and 8. Infrared scanning and phase change paint thermal mapping techniques were used to determine smooth wall turbulent and laminar heating levels and localized heating effects due to protuberances. Protuberances included a scaled raceway, lateral support pad shear tabs, and stage II roll control jets. The flowfield about the missile during the stage I/stage II separation event was investigated using a cold gas simulation of the stage II motor plume. Measured smooth wall heating rates confirmed both laminar and turbulent theoretical predictions and significant heating augmentation in excess of five times the smooth wall values was found in the vicinity of the leading edge of the raceway and the shear tabs. An extensive interaction region was produced by the roll control system jets. Schlieren photography of the staging event showed plume induced flow separation extending to the nose of the missile.

Nomenclature

A	= area
A_{ref}	= missile reference area
D_m	= missile or model cross-sectional diameter
h	= heat-transfer coefficient (see Eq. 1), Btu/ft^2-s-°R
hi/hu	= ratio of interference heating to undisturbed heating
i.r.	= infrared camera view
ℓ	= model or missile length
M	= Mach number
p	= static pressure
P_t	= tunnel total pressure
$\dot{q}$	= convective heat-transfer rate
q	= dynamic pressure
RCS	= roll control system
Re_ℓ	= freestream Reynolds number based on missile or model length
Re/ft	= unit freestream Reynolds number
S	= stage separation distance
T_r	= recovery temperature
T_t	= tunnel total temperature
T_w	= model wall (surface) temperature
α	= model angle of attack
γ	= ratio of specific heats

Subscripts

e	= stage II nozzle exit
ℓ	= local external flow over missile or based on model/missile length
∞	= undisturbed freestream

Introduction

THIS paper presents preliminary results of recently completed wind tunnel tests to determine aerodynamic heating patterns and general flowfield characteristics of the MX missile. The qualitative flowfield effects of the stage I/stage II separation event were also investigated. The tests were conducted at Mach numbers of 6 and 8.

The purpose of the tests was to provide early data to define potential problem areas associated with MX ascent flight. The areas of interest included triconic shroud heating, raceway and shear tab protuberance heating, stage II roll control system heating and flowfield effects, and I/II staging flowfield effects.

Thermal mapping was accomplished through the use of infrared scanning and phase change paint techniques. Flowfield analysis was accomplished qualitatively from phase change paint, shadowgraph, and schlieren photographic data. The results obtained are being used to define missile design requirements and future wind tunnel test requirements.

Model Description

Two models were tested: one a 5% scale model of the full missile (Fig. 1); and the other a 12.5% scale model of the forward end of the missile including the shroud, stage IV, and a portion of stage III (Fig. 2). The 5% model had provision for gas flow to simulate the staging gas dynamics and to supply the four roll control nozzles. Stage I was moveable axially in fixed increments to simulate staging and completely removeable for simulating stage II flight. Solid plume simulators were provided for stage I and stage II motors. The model also had scaled lateral support pad shear tabs and raceway. The 12.5% model, designed primarily for thermal mapping, included three shear tab heights to investigate the effect of tab height on local heating augmentation. Simulated 1/8 in., 1/2 in., and 1 in. tab heights were modeled. The outer surface of the models consisted of RTV rubber which was cast over a machined steel core. The RTV provided a surface of low thermal diffusivity which is a requirement for the use of infrared scanning and phase change paint techniques.

Test Program

MX flight at Mach 6 and 8 was simulated with both models in the AEDC von Kármán Facility, Tunnel B.[1] Figure 3 shows the Mach number vs Reynolds number simulation capabilities of this tunnel along with the full scale flight profile. The conditions tested are given in Table 1. Figure 3 also indicates the approximate location for boundary layer transition based on flight and wind tunnel measurements presented in Ref. 2. The shaded area encompasses the trends of the beginning and end of transition.

Presented as Paper 80-1310 at the AIAA/SAE/ASME 16th Joint Propulsion Conference, Hartford, Conn., June 30-July 2, 1980; submitted Oct. 20, 1980; revision received Oct. 2, 1981.

*Senior Group Engineer, Engineering Mechanics Department, Thermophysics Section. Member AIAA.

†Staff Engineer, Engineering Mechanics Department, Thermophysics Section. Associate Fellow AIAA.

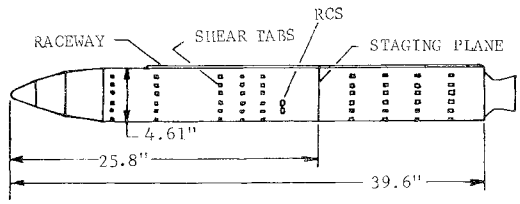

Fig. 1 5% scale MX model.

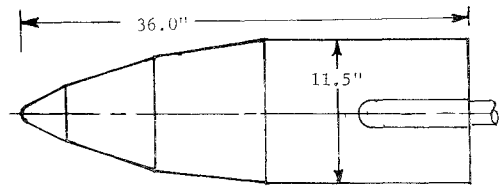

Fig. 2 12½% scale MX model.

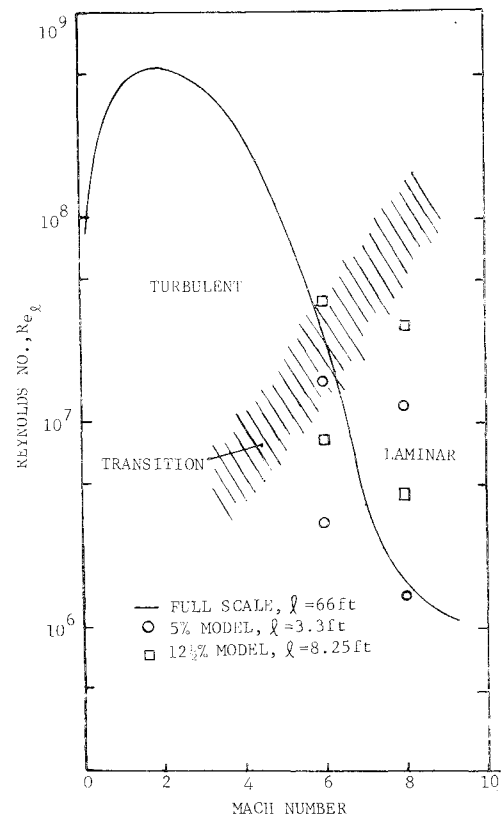

Fig. 3 Reynolds number vs Mach number characteristics.

The use of infrared scanning and phase change paint techniques for measuring aerodynamic heating rates is well documented.[3,4] Briefly, in the infrared technique a scanning camera is used to detect radiation from the model surface in the wavelength range of 3-5.8 μm. The energy detected from a known area on the surface (spot) is digitized and converted to an average surface temperature using known radiation laws.[3]

In the phase change paint technique the model is sprayed with a paint containing a fine emulsion of wax having a known melting point. As the model heats up in the tunnel flow the wax melts wherever the surface temperature reaches the melting point. At any time then, the observed (photographically recorded) melt lines indicate isotherms of known temperature.

Once the surface temperature is known, the heat-transfer coefficient, h, is determined in both techniques by a solution of the one-dimensional, unsteady conduction equation for a semi-infinite slab.[4] For a model whose thickness is not infinite, the semi-infinite slab assumption is valid as long as the thermal diffusivity of the model material is low. Thus the model is made from rubber-like materials such as RTV.

Table 1 Test conditions

Mach no.	P_t, psia	T_t, °F	Re/ft $\times 10^{-6}$
5% Model			
6	50	390	1.0
6	270	390	4.9
8	60	770	0.3
8	850	880	3.7
12.5% Model			
6	50	390	1.0
6	270	390	5.0
8	96	840	0.5
8	850	890	3.7

Table 2 Staging mass flow conditions

S/D_m	Nozzle mass flow, lbm/s
0.0326	0.84
0.0652	1.11
0.0978	1.32
0.125	1.56
0.250	2.18
0.375	2.62
0.500	3.04

The staging event between stage I and stage II of the missile was simulated by making a series of runs at Mach 6 with the two stages separated at predetermined intervals. At each separation the stage II motor exhaust was simulated with a cold gas jet whose thrust was consistent with the separation distance. The scaling used for this simulation is discussed in the Appendix. Table 2 gives the separation distances and mass flows tested.

5% Model Results

Representative infrared scanning data from the 5% model are illustrated in Figs. 4-7. These figures show measured heat-transfer coefficients along the centerline of the model's upper surface. The model was rolled to get the various protuberances onto the upper centerline and thus into normal view of the infrared camera. The cross-sectional views on each figure indicate the various roll orientations for the i.r.

The heat-transfer coefficients presented in this paper have been defined in terms of the tunnel stagnation temperature. That is,

$$h = \dot{q}/(T_t - T_w). \tag{1}$$

Ordinarily, and more fundamentally, a local recovery temperature, T_r, would be used in defining the heat-transfer coefficient. However, recovery temperatures were not measured during these tests. Use of T_t in Eq. (1) allowed a consistent set of data to be presented and eliminated the uncertainties in analytically predicting the variation of T_r over the surface. Caution, however, must be used in comparing these data to other data or predictions. For example, heat-transfer coefficients based on a recovery-to-stagnation temperature ratio of 0.9 would be as much as 28% higher than presented here at Mach 6.

Figure 4 shows two scans at zero angle of attack. The upper curve is along the raceway. Both curves show natural tran-

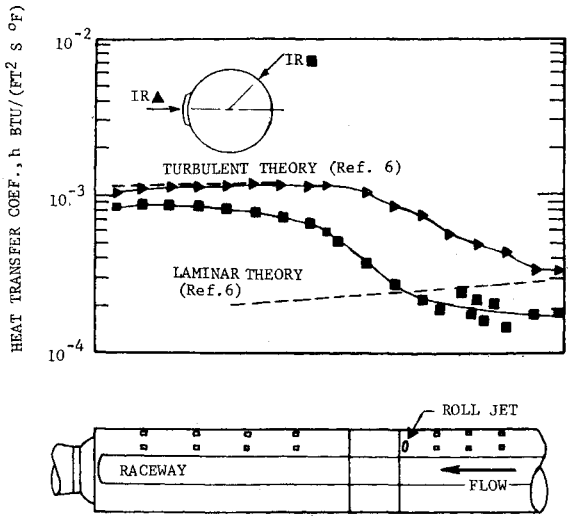

Fig. 4 Boundary layer transition on 5% scale model: $M=6$, $\alpha=0$, $Re/ft=5\times10^6$.

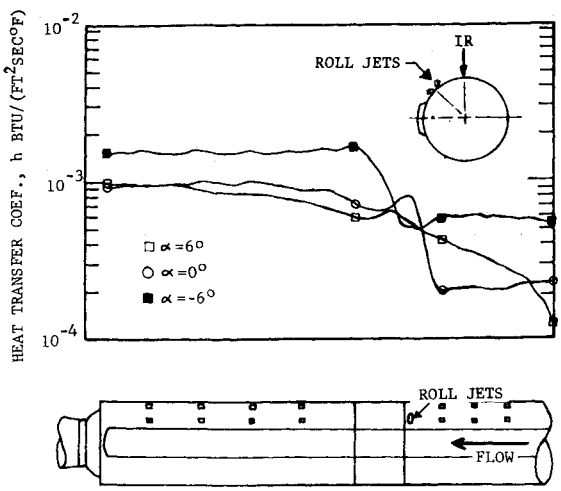

Fig. 5 Effect of angle of attack on heating rate: $M=6$, $Re/ft=5\times10^6$.

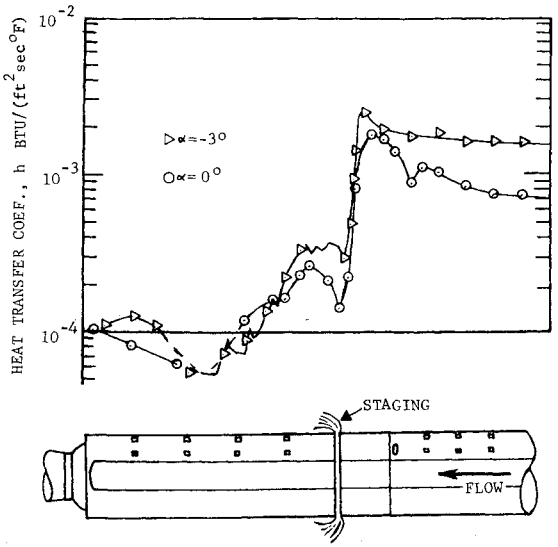

Fig. 6 I/II staging: $S/D_m=0.0326$, $M=6$, $Re/ft=5\times10^6$.

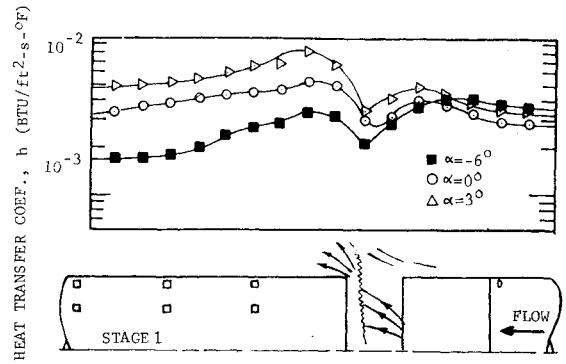

Fig. 7 I/II staging: $S/D_m=0.3750$, $M=6$, $Re/ft=5\times10^6$.

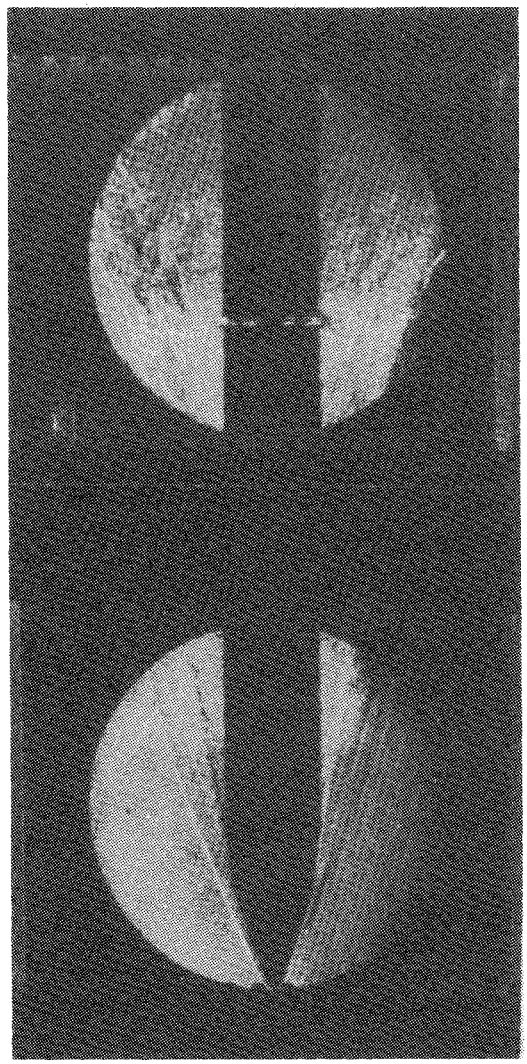

Fig. 8 Schlieren photo of staging: $S/D_m=0.0326$, $M=6$.

sition about halfway down the model. The leading edge of the raceway (not in view) apparently induces earlier transition and subsequently higher heating rates. The unsteadiness in the laminar data on the lower curve may be due to the perturbing influence of the shear tabs on the transition process. Reference to Fig. 3 shows that a similar transition situation can be anticipated in full scale MX flight at Mach 6.

Angle of attack effects are pointed out in Fig. 5. Note that for positive angles of attack the infrared camera views the leeward side of the model, while at negative angles of attack the windward is viewed. As expected, the windward heating is higher than the leeward. The abrupt transition for the $\alpha=0$

and −6 deg cases is not completely understood, but it is suspected to be due to the presence of the tangentially directed roll jet. The significant circumferential effect of the RCS is discussed later.

Figures 6 and 7 show the effects of the staging event on the flow over the forward and aft stages. Figure 6 corresponds to early in the staging event and shows a blanketing effect of the staging gas on the aft stage. Figure 7 corresponds to late in the staging event when the flow is apparently re-establishing itself over the aft stage. In both cases heating on the forward stage is significantly increased due to staging. Figures 8 and 9 are schlieren photographs of the staging event. The staging gas plume is seen to induce flow separation forward to the nose of the model.

The effect of the roll control jets at Mach 6 is shown by the oil flow patterns in Fig. 10. A strong local effect near the nozzles is indicated, as well as a significant downstream influence.

Figure 11 is a heating contour plot for one jet at Mach 6 and 3 deg angle of attack. The contours were traced from successive phase change paint photos. The plot is slightly distorted due to model curvature and an oblique camera angle. Protuberance type heating is in evidence on the surface upstream of the jet. High heating is also seen confined to narrow regions swept downstream to either side of the jet. The high heating is probably due to a horseshoe-like vortex similar to that observed about solid protuberances.

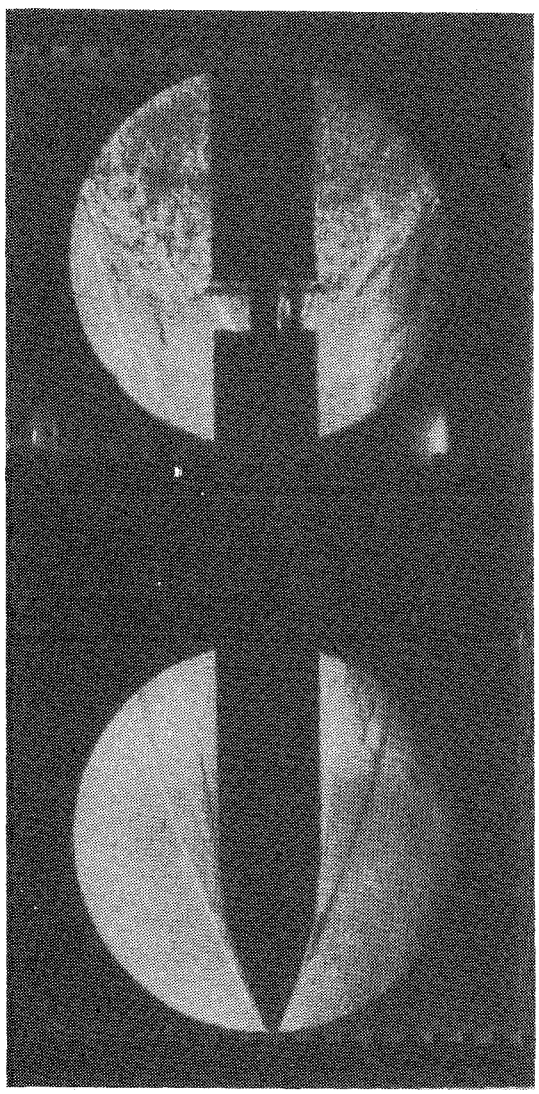

Fig. 9 Schlieren photo of staging: $S/D_m = 0.500$, $M = 6$.

12½% Model Results

Figures 12-14 show typical infrared scanning data for the 12½% model. Figure 12 shows the need for tripping the flow to produce a turbulent boundary layer. The trip consisted of two 0.020 in. wires twisted together and attached to the middle of the second cone of the nose. The twisted wire technique has been used by the second author on several test programs and appears to be a reliable method of fixing transition. The simplicity of installation and removal is

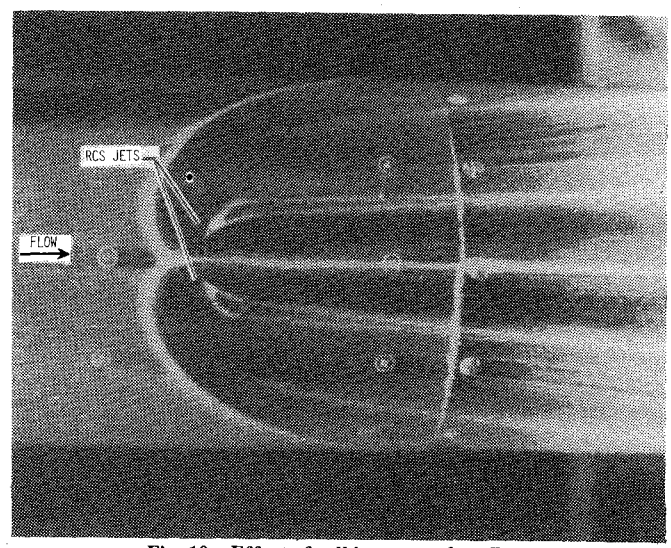

Fig. 10 Effect of roll jets on surface flow.

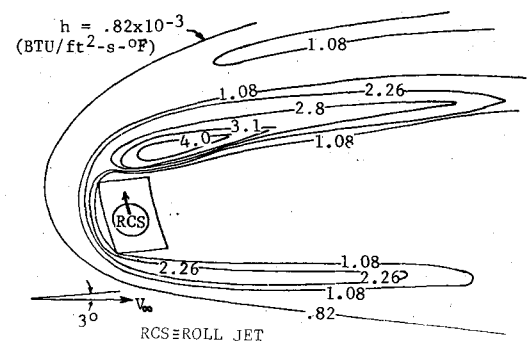

Fig. 11 Contour plot of heating due to roll jet: $M = 6$, $\alpha = -3$ deg, $Re/ft = 5 \times 10^6$.

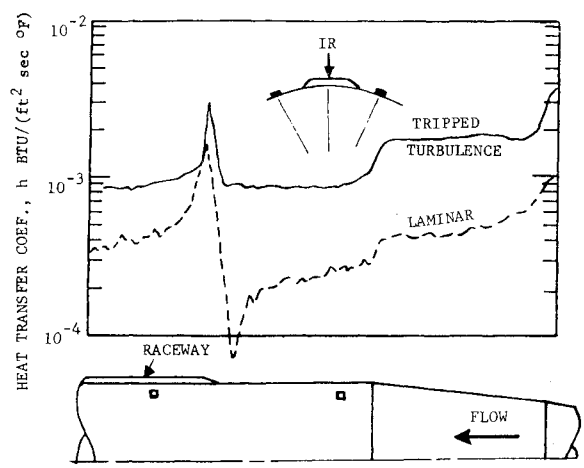

Fig. 12 Effect of boundary layer trip: $M = 6$, $\alpha = 0$, 12½% model, $Re/ft = 5 \times 10^6$.

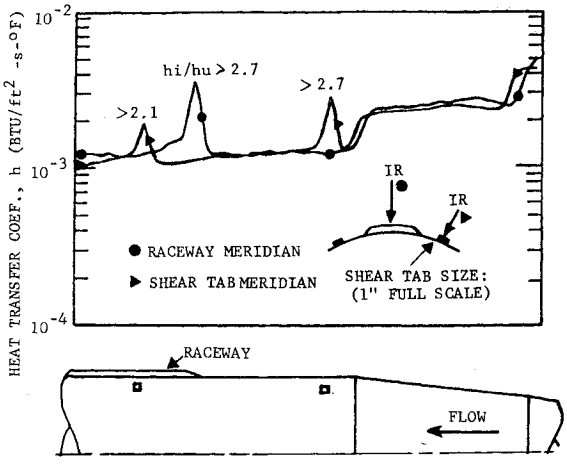

Fig. 13 Raceway and shear tab heating: $M=6$, $\alpha=-6$ deg, $Re/ft=5\times10^6$.

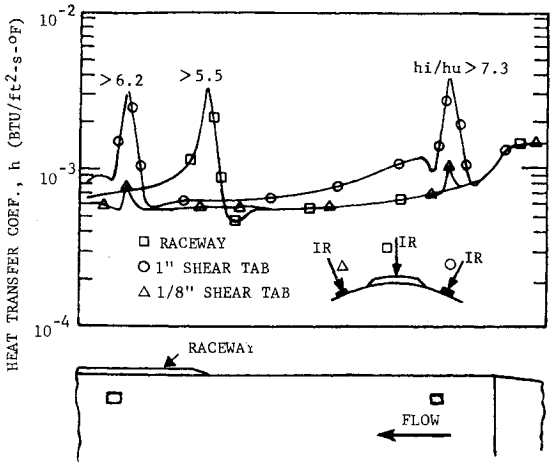

Fig. 14 Raceway and shear tab heating: $M=8$, $\alpha=0$, $Re/ft=3.7\times10^6$.

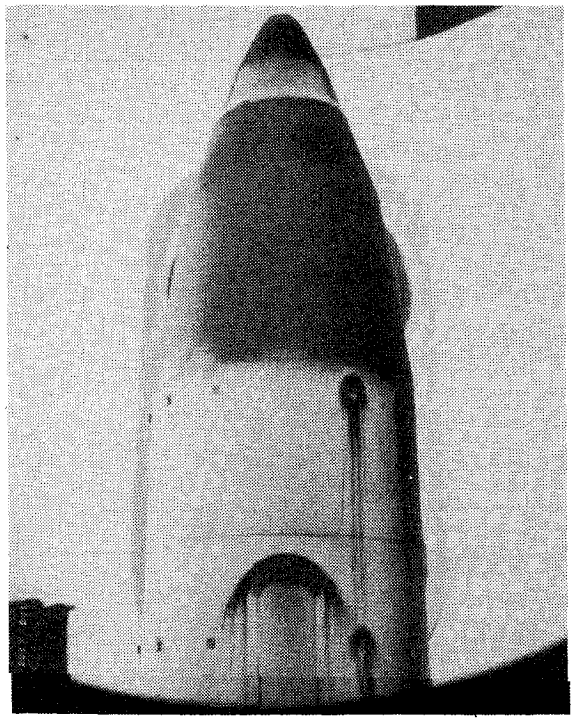

Fig. 15 Phase change paint photo of protuberance heating: $M=6$, $\alpha=0$.

particularly attractive when various trip locations and heights are being investigated.

As with the 5% model, reference to Fig. 3 shows that transitional conditions were to be expected, both for the tests and in full scale flight.

Figures 13 and 14 show the localized heating effects due to the raceway leading edge and the shear tabs. The values of interference heating shown on these figures are given only as lower bounds. The resolution associated with the infrared system and the model scale used in these tests is such that high-temperature gradients are averaged and the temperature at the protuberance, computed from the measured radiant energy, is lower than the maximum temperature at the protuberance. Peak heat-transfer coefficients may be considerably higher than indicated in the figures.

Further evidence of localized heating is shown in Fig. 15 which is a photograph of a phase change paint run at Mach 6. The dark regions are melted paint and thus represent "hot" areas. Figure 16 is a contour plot of heating near the raceway leading edge. Figure 17 is a contour plot of heating at the shear tabs. The higher heating induced by the larger tabs is apparent from these plots.

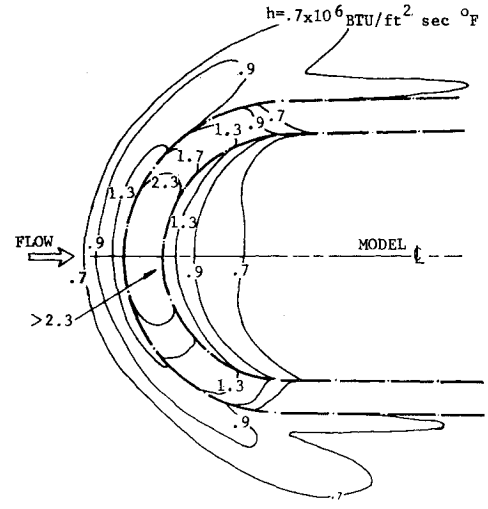

Fig. 16 Contour plot of heating due to raceway: $M=6$, $\alpha=0$, $Re/ft=5\times10^6$.

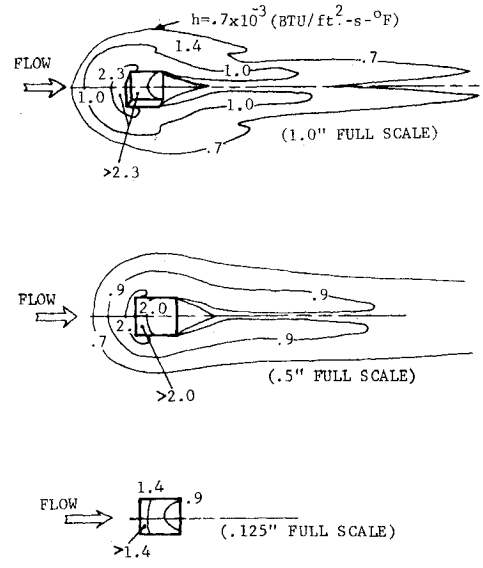

Fig. 17 Contour plot of heating due to shear tab: $M=6$, $\alpha=0$, $Re/ft=5\times10^6$.

Concluding Remarks

Preliminary tests have revealed several interesting and significant features of the convective heating and flow over the MX missile:

1) Natural transition occurred about halfway down the 5% model at Mach 6. This is consistent with predicted transition in full scale flight. Boundary layer trips were required for fully turbulent flow over both models at Mach 6 and Mach 8.

2) At Mach 6, heating along the raceway (far from the leading edge) was higher than along the missile surface. This was true for both laminar and turbulent flow.

3) The roll jets acted like protuberances to produce high local heating near the jet exits. Interaction of the roll jets and the missile flowfield produced enhanced heating downstream over the stage I cylinder.

4) High local heating rates were observed at the raceway leading edge and the larger (½ in. and 1 in. full scale) shear tabs. Values of *hi/hu* were not accurately determined, but are bounded from below by $hi/hu = 3$ at Mach 6 and $hi/hu = 6$ at Mach 8.

5) The staging event has a significant effect on the flow over the missile. Flow separation was observed over the forward stages all the way to the nose shroud.

Appendix

During the stage I/stage II separation the important external flow phenomena are governed by the interaction of the exhaust gas issuing from the circumferential gap between stages and the local freestream flow. This interaction was modeled by equating the ratios of stage II nozzle momentum flux to freestream momentum flux of the model and full scale vehicle.[5] Based on the local freestream dynamic pressure and a representative area, say $A_{ref} = \pi D_m S$, we have

$$\left[\frac{p_e M_e^2 A_e}{q_\ell D_m S}\right]_{\text{Model}} = \left[\frac{p_e M_e^2 A_e}{q_\ell D_m S}\right]_{\text{Full Scale}} \tag{A1}$$

In addition, the nozzle exit-to-local freestream pressure ratios were matched. That is,

$$\left(\frac{p_e}{p_\ell}\right)_{\text{Model}} = \left(\frac{p_e}{p_\ell}\right)_{\text{Full Scale}} \tag{A2}$$

At the staging plane, $p_\ell \approx p_\infty$ and Eq. (A1) can be rewritten as

$$\left[\frac{p_\infty M_e^2 A_e}{q_\ell}\right]_{\text{Model}} = \frac{(D_m S)_{\text{Model}}}{(D_m S)_{\text{Full Scale}}} \cdot \left[\frac{p_\infty M_e^2 A_e}{q_\ell}\right]_{\text{Full Scale}} \tag{A3}$$

If the stage separation is scaled with diameter, i.e., if $(S/D_m)_{\text{Model}} = (S/D_m)_{\text{Full Scale}}$, then $[(D_m S)_{\text{Model}}]/[(D_m S)_{\text{Full Scale}}]$ is simply the square of the model scale factor, $(0.05)^2$.

All of the quantities on the right-hand side of Eq. (A3) are known as is $(p_\infty/q_\ell)_{\text{Model}}$ on the left-hand side. The model nozzle exit area, A_e, was chosen on the basis of model design constraints leaving only the model nozzle exit Mach number to be calculated from Eq. (A3). This fixed the model nozzle throat area.

The full scale nozzle exit pressure, p_e, is a function of the stage separation distance, S, and was determined from full scale staging simulations. The model exit pressure is obtained then from Eq. (A2). With p_e known, the required mass flows were computed as a function of the stage separation distance.

A similar procedure was used to model the roll control nozzle flows.

Acknowledgments

This work was sponsored by the Department of the Air Force, Ballistic Missile Office under Contract F04704-78-C-0016. The authors also acknowledge the contributions of Messrs. D.W. Stallings and K.W. Nutt of Calspan Corp., Tullahoma, Tenn.

References

[1] "Test Facilities Handbook (Eleventh Ed.)," Arnold Engineering Development Center, Arnold Air Force Station, Tenn., June 1979.

[2] Rubesin, M.W., Rumsey, C.B., and Varga, S.A., "A Summary of Available Knowledge Concerning Skin Friction and Heat Transfer and Its Application to the Design of High Speed Missiles," NACA RM A51J25a, Nov. 6, 1951.

[3] Boylan, D.E., Carver, D.B., Stallings, D.W., and Trimmer, L.L., "Measurement and Mapping of Aerodynamic Heating Using a Remote Infrared Scanning Camera in Continuous Flow Wind Tunnels," AIAA Paper 78-799, April 1978.

[4] Jones, R.A. and Hunt, J.L., "Use of Fusible Temperature Indicators for Obtaining Quantitative Aerodynamic Heat-Transfer Data," NASA-TR-R-230, Feb. 1966.

[5] Romine, G.L., private communication, Martin Marietta Corp., Jan. 1980.

[6] Tong, H., "Nonequilibrium Chemistry Boundary Layer Integral Matrix Procedure, Part I (BLIMPK)," Aerotherm Report UM-73-37, July 1973.